Electrically Controllable Spontaneous Magnetism in Nanoscale Mixed Phase Multiferroics

Q. He[1], Y. H. Chu[2], J. T. Heron[3], S. Y. Yang[1], C. H. Wang[2], C. Y. Kuo[4], H. J. Lin[4], P. Yu[1], C. W. Liang[2], R. J. Zeches[3], C. T. Chen[4], E. Arenholz[5], A. Scholl[5], and R. Ramesh[1,3,6]

[1] Department of Physics, University of California, Berkeley, CA 94720, USA

[2] Department of Materials Science and Engineering, National Chiao Tung University, Hsinchu 30010, Taiwan, R.O.C.

[3] Department of Materials Science and Engineering, University of California, Berkeley, CA 94720, USA

[4] National Synchrotron Radiation Research Center, Hsinchu 30076, Taiwan, R.O.C.

[5] Advanced Light Source, Lawrence Berkeley National Laboratory, Berkeley, CA 94720, USA

[6] Materials Science Division, Lawrence Berkeley National Laboratory, Berkeley, CA 94720, USA

Abstract:

The emergence of enhanced spontaneous magnetic moments in self-assembled, epitaxial nanostructures of tetragonal (T-phase) and rhombohedral phases (R-phase) of the multiferroic $BiFeO_3$ system is demonstrated. X-ray magnetic circular dichroism based photoemission electron microscopy (PEEM) was applied to investigate the local nature of this magnetism. We find that the spontaneous magnetization of the R-phase is significantly enhanced above the canted antiferromagnetic moment in the bulk phase, as a consequence of a piezomagnetic coupling to the adjacent T-phase and the epitaxial constraint. Reversible electric field control and manipulation of this magnetic moment at room temperature is shown using a combination of piezoresponse force microscopy and PEEM studies.

The ability to use epitaxy as a tool to control the ground state of a material has enabled the discovery of a wide range of new phenomena in modern materials[1,2]. In a recent paper[3], large compressive epitaxial strains were imposed on the rhombohedral phase (R-phase) multiferroic, $BiFeO_3$, to stabilize a tetragonal-like phase (T-phase) with a significantly large c/a ratio. It was also demonstrated that partial relaxation of this epitaxial strain leads to the formation of a nanoscale mixture of the T- and R-phases, thus resembling a classical morphotropic phase boundary in modern piezoelectrics[4,5]. Over the past two decades, novel physical phenomena have emerged in complex oxides, at interfaces that are naturally created within the system (e.g., phase-separated manganites, relaxor ferroelectrics), or in artificially engineered heterostructures[6,7,8,9,10,11]. Although much of these phenomena have emerged as a consequence of chemical substitutions, strain control is emerging as an equally powerful tool to create and manipulate such phenomena[2]. With this as the backdrop, in this study we describe a novel approach to create a magnetic state and the ability to electrically control this emergent magnetism at room temperature. An enhanced spontaneous magnetic moment arises in the R-phase that is strain confined between T-phases. Due to the local nature of this magnetism, we have used X-ray magnetic circular dichroism based photoemission electron microscopy (XMCD-PEEM)[12,13] to investigate the magnetism. In combination with electrical control of the local ferroelectric state, we demonstrate that this local magnetic moment can be erased by the application of an electric field. Finally, reversal of the electric field polarity restores the mixed phase structure.

The samples were prepared using pulsed laser deposition in conjunction with high-pressure reflective high-energy electron diffraction to monitor the growth of the BFO thin films. A bottom conducting layer of $LaNiO_3$ was inserted in order to eliminate the charging effects during X-ray

illumination. Partial strain relaxation through control of the film thickness leads to the formation of two orthogonal arrays of nanoscale, T+R phase mixtures, as illustrated in the AFM image in Figure 1(a). The individual stripe-like regions, Figure 1(b), consist of a nanoscale ensemble of T- and R-phases with a characteristic length scale of 20-40nm. The graph on the bottom of this figure shows a cross-sectional line-profile of the mixed phase area, revealing two different tilting angles (2.8° and 1.6°) of the mixed phase features. The structural details of such a mixed phase ensemble were identified from careful X-ray 2θ-ω scans, such as that shown in Figure 1(c). The R-phase and T-phase are labeled as R and T respectively. The X-ray data also identifies the structural distortion of the R-phase, with out-of-plane lattice parameter of (c=4.17Å); this coupled with reciprocal space maps provides a measure of the in-plane dimensions of this highly strained R-phase to be 3.82 Å. From the four peaks arising from the R-phase, Figure 1(c), the tilt angles for these can be divided into two groups, one ~2.8 °and the other ~0.6°, which correspond to the green and red shaded area in Fig. 1(a). The broadening angle for the T-phase (c=4.64Å) is estimated to be 1.6°, resulting from the tilting of the T-phase, consistent with the AFM measurement. Compared to the AFM line profile, we find that the R-phase with a tilt angle of 2.8° is on the other side of the peaks to the T-phase. Therefore, we can locate the R- and T-phases with the slopes of the topography shown in Fig. 1(b) and schematically illustrated in Fig.1 (d). The AFM and X-ray diffraction studies clearly establish the nanoscale, R-T mixed-phase ensemble, in which the R-phase is highly strained compared to the bulk. Since BFO in the bulk is a well-known ferroelectric and canted antiferromagnet [14,15,16], it is natural to ask: what is the magnetic state of the mixed phase BFO, especially in the highly strained R-phase?

X-ray magnetic circular dichroism (XMCD) is a powerful method to study the magnetic response of a material[17,18]. We have employed this technique to explore the magnetic response of

BFO films with mixed phases, and compared to unconstrained R-and pure T-phase films. X-ray absorption spectra (XAS) at Fe^{3+} $L_{2,3}$-edge using left and right circularly polarized soft X-rays, at grazing incidence ($\theta = 30°$) were obtained as a function of the external magnetic field. Then the XMCD spectra were measured in two complementary ways. Figure 2(a) shows the XMCD signal obtained from the difference between XAS in positive and negative (parallel and antiparallel to the *k*-vector of the incident X-ray) magnetic field (+/- 2 T) and fixed X-ray polarization. Figure 2(b) is the XMCD spectra extracted from the difference between XAS with left and right circularly polarized X-rays in a constant 4 T magnetic field. The red curve in Figure 2(a) is from a pure rhombohedral phase BFO sample, which gives a relatively negligible XMCD signal (since the canted moment is only ~6-8 emu/cc)[14]. No canting of Fe^{3+} spins is allowed in the tetragonal phase BFO due to symmetry and thus, it does not exhibit any XMCD (data in green in Figure 2(a,b))[19]. The significantly larger XMCD spectra of mixed T+R phase BFO ensembles are shown as the black curves in Figure 2(a,b), indicating that a higher magnetic moment is present in mixed phase BFO films. The XMCD spectra in Figure 2(a) are measured with left circularly polarized (LCP) X-rays; they reverse polarity when using right circularly polarized (RCP) X-rays, confirming that the response is magnetic in origin. Both these complementary measurements clearly reveal the existence of a spontaneous magnetic moment in the mixed phase samples. From the ~1% XMCD signal, and using data for other oxide systems (manganites, Fe_3O_4)[20,21,22,23] as a semi-quantitative calibration, we estimate the magnetization to be of the order of 30-40 emu/cc. In order to explore the microscopic origins of this enhanced magnetic moment, the XMCD signal was imaged using photoemission electron microscopy (PEEM).

Spatially resolved PEEM images were obtained using both LCP and RCP incident X-rays at a grazing incidence angle ($\theta = 30°$). To enhance the difference in the magnetic contrast and eliminate the contribution from the topographic contrast, the ratio of the two images was taken. The image contrast is effectively a map of the local magnetization vector; regions that have their magnetic moment lying parallel to the X-ray wave vector show bright contrast, while those that are antiparallel appear in dark contrast. Angle-dependent XMCD-PEEM images were taken with the incident X-rays at various orientations ($\phi = 0°$, 90°, 180°), shown schematically in Figure 3(a). Figure 3(b) is the PEEM image obtained by LCP X-ray at $\phi = 0°$, showing mainly topographic contrast. The darker areas in this image are in the valleys of the mixed phase features and brighter areas are at the peaks. The XMCD image, (Figure 3(c)), reveals the intrinsic magnetic contrast that appears as bright and dark stripe-like patterns indicating that these stripes have magnetic moments lying parallel and antiparallel to the incident X-rays. When the sample is rotated by 180°, all of the stripes reverse contrast, which further confirms the magnetic origin, Figure 3(c). Moreover, after a 90° rotation of the sample about the sample normal, the stripes show weak or no contrast when the incident X-ray is perpendicular to their long axes; at the same time, the stripes show strongest contrast when the incident X-ray is parallel to their long sides (Figure 3(b)). These measurements clearly indicate that the magnetic moments in the stripe-like area are lying along the long axis of the stripes. It is also important to note that the regions in bright and dark magnetic contrast in Figure 3(b) are approximately of equal fractions.

To further explore the origins of the magnetic response, we focus on the lower red, boxed area in Figure 3(c) and compare with both the AFM line scans and the corresponding piezo-response force microscopy (PFM) images of the same area. Figure 4(a) is the AFM topography image and the corresponding in-plane PFM image acquired simultaneously at exactly the same

position is shown in Figure 4(b). The PFM image shows bright contrast of "lip-shaped" patterns surrounding the stripe-like features. By obtaining a line profile across the mixed phase features, the topography curve (black curve in Figure 4(d)) shows a significant asymmetry of slopes on phase on the two sides of the rhombohedral phase similar to what was shown in the cross sectional AFM line profile in Figure 1(b). Combining the in-plane PFM line profile (green curve in Figure 4(d)) with the topology scan helps us to conclude that the lip-shaped patterns form the T/R interface. More importantly, the area enclosed by the "lip-shaped" region is on the steeper side, which is the R-phase as shown in Figure 1(b). The corresponding magnetic information of the same area is obtained from the zoomed-in XMCD-PEEM image, Figure 4(c). By superimposing the PEEM and PFM line profiles together in Figure 4(d), it is clear that this highly distorted R-phase is the source of the enhanced magnetic moment in the XMCD image, arising from a piezomagnetic effect[24,25,26].

Conventional SQUID magnetometry of these samples did not yield a significantly enhanced moment compared to the canted moment of the R-phase. Although puzzling at the outset, this apparent inconsistency can be understood from a closer examination of the PEEM data in Figure 3(b), which shows an approximately equal fraction of bright and dark stripes (i.e., regions of anti-parallel magnetization) in most samples. It is our strong surmise that these stripes are not ferromagnetic; instead we believe they are pyromagnetic, with the magnetic moment strongly coupled and pinned to the lattice. Thus, in order to independently verify the existence of this pyromagnetic moment we explored the exchange coupling of this moment to a ferromagnetic layer.

2.5 nm thick, ferromagnetic $Co_{.90}Fe_{.10}$ (CoFe) thin films were deposited onto BFO films containing a large fraction of mixed phase regions at room temperature by DC magnetron

sputtering in a UHV system of base pressure of ~5 x 10^{-8} Torr. The CoFe films were capped with a 2 nm thick layer of Pt to prevent its oxidation. A uniform magnetic field of 200 Oe was applied during the CoFe growth to set the uniaxial anisotropy direction. Then, Co-edge XMCD-PEEM imaging was employed in different orientations (Φ=0°, 45°, 90°, 180°) to investigate the ferromagnetic domain structures in CoFe layer. Figure 5(a) is taken with LCP X-rays, which clearly shows us the topography of mixed phase structure covered by CoFe that was grown in an applied magnetic field along 1 10] direction. Bar-shaped magnetic domains can be seen in the XMCD-PEEM images (Figure 5(b)-(e)). It is interesting to note that the bar-shaped domain patterns in these magnetic images strongly resemble the corresponding bar-shaped patterns (identified within the red box and schematically depicted in Figure 5(f)) in the topographic image in Figure 5(a). 5(b) was taken with circularly polarized X-rays incident from [100] direction, which shows horizontal bar-shaped domains in dark contrast while vertical bar-shaped domains appear in neutral (gray) contrast, indicating that the magnetization of CoFe in the horizontal and vertical domains are pointing antiparallel ([0 10]) and perpendicular ([100] or 100]) to the incident X-rays, respectively. This magnetization direction coupled with the moment in the mixed phase features (along the long side of the mixed phase stripes but the short side of the CoFe domains), which is also schematically shown in Figure 5(f). When we rotate the sample by 45° with respect to the sample normal, the XMCD amplitude from the CoFe domains decreases by about a factor of $\bar{}$, reflecting the reduced contrast in the PEEM image shown in Figure 5(c). This confirms our interpretation of the moment directions. With a 90° rotation of the sample, the change of contrast of XMCD-PEEM image (Figure 5(d)) suggests that the moments in the vertical CoFe domains lie along [100] direction. Finally, a 180° rotation of the sample gives us a fully reversed contrast image (Figure 5(e)), confirming the contrast we observed here is indeed

magnetic in origin and that the moments in the CoFe layer are magnetically coupled to the moment in the R-phase of the BFO underlayer[27]. This robust magnetic coupling provides additional evidence on the existence of magnetic moments embedded in R-phase of the mixed phase nanostructures in BFO.

Having established the existence of a nanoscale magnetic moment in the highly distorted R-phase, we demonstrate the electric field modulation of this magnetism. By applying a +24V DC bias to a PFM tip and scanning over the red rectangular area (Figure 6(a)), the mixed phase features can be transformed into pure tetragonal phase. Then, applying a -8V DC bias to the green rectangular area, the mixed phase features return. LCP and XMCD-PEEM images of this area are shown in Figure 6. By mapping the magnetic moments (XMCD image), no magnetic contrast is observed in the area between the green and red boxes, consistent with the non-magnetic state of tetragonal phase. In contrast, the XMCD images show the characteristic stripe-shaped features both inside the green box and outside the red box area, indicative of a magnetic moment in them. Therefore, we conclude that magnetic moments in these stripe-shaped nanoscale mixed phase regions can be erased and rewritten at room temperature with only the application of an electric field.

In summary, we have demonstrated a novel approach to manipulate the canted moment of the R-phase of $BiFeO_3$, by creating a nanoscale ensemble in which the R-phase is mechanically confined by regions of the T-phase. This nanoscale mixture displays functional responses that are strikingly different from the parent phases, thus embodying the spirit of a morphotropic phase boundary in a relaxor ferroelectric or the electronically phase separated scenarios in the CMR manganites. Detailed analyses using a combination of experimental probes reveal that the enhanced magnetic moment resides within the distorted R-phase rather than at the interfaces.

The strong coupling to the underlying lattice is a primary reason that this moment is not switchable with a magnetic field; in contrast, it can be controlled by electric fields that making it a novel vehicle to demonstrate magnetoelectric coupling and electric field control of magnetism in this multiferroic system. Deterministic control of the location, size and distribution of this mixed phase ensemble would be a critical enabler of approaches to use the results of this study in future magnetoelectronic applications.

This work was supported by the Director, Office of Science, Office of Basic Energy Sciences, of the U.S. Department of Energy under Contract No. DE-AC02-05CH11231.

References:

[1] Schlom, D. G. *et al.* A thin film approach to engineering functionality into oxides. *J. Am. Ceram. Soc* **91**, 2429 (2008).

[2] Choi, K. J. *et al.* Enhancement of ferroelectricity in strained $BaTiO_3$ thin films. *Science* **306**, 1005 (2004).

[3] Béa, H. *et al.* Evidence for room-temperature multiferroicity in a compound with a giant axial ratio. *Phys. Rev. Lett.* **102**, 217603 (2009).

[4] Zeches, R. J. *et al.* A strain-driven morphotropic phase boundary in $BiFeO_3$. *Science* **326**, 977 (2009).

[5] Chen, Z. *et al.* A strain-driven morphotropic phase boundary in $BiFeO_3$. *Appl. Phys. Lett.* **96**, 252903 (2010).

[6] Fu, H. and Cohen, R. E. Polarization rotation mechanism for ultrahigh electromechanical response in single-crystal piezoelectrics. *Nature* **403**, 281 (2000).

[7] Chakhalian, J. *et al.* Orbital reconstruction and covalent bonding at an oxide interface. *Science* **318**, 1114 (2007).

[8] Ohtomo, A. and Hwang, H. Y., A High mobility electron gas at the $LaAlO_3/SrTiO_3$ heterointerface. *Nature* **427**, 423 (2003).

[9] Reyren, N. *et al.* Superconducting interfaces between insulating oxides. *Science* **317**, 1196 (2007).

[10] Yu, P. *et al.* Interface ferromagnetism and orbital reconstruction in $BiFeO_3$-$La_{0.7}Sr_{0.3}MnO_3$ heterostructures. *Phys. Rev. Lett.* **105**, 027201 (2010).

[11] Garcia-Barriocanal, J. *et al.* Colossal ionic conductivity at interfaces of epitaxial ZrO_2: $Y_2O_3/SrTiO_3$ heterostructures. *Science* **321**, 676 (2008).

[12] Nolting, F. *et al.* Direct observation of the alignment of ferromagnetic spins by antiferromagnetic spins. *Nature* **405**, 6788 (2000).

[13] Scholl, A. *et al.* X-ray photoemission electron microscopy, a tool for investigation of complex magnetic structures. *Rev. Sci. Instrum.* **73**, 1362 (2002).

[14] Ederer, C. and Spaldin, N. A. Weak ferromagnetism and magnetoelectric coupling in bismuth ferrite. *Phys. Rev. B* **71**, 060401 (2005).

[15] Lebeugle, D. *et al.* Room-temperature coexistence of large electric polarization and magnetic order in $BiFeO_3$ single crystals. *Phys. Rev. B* **76**, 024116 (2007).

[16] Lebeugle, D. *et al.* Electric-field-induced spin flop in $BiFeO_3$ single crystals at room temperature. *Phys. Rev. Lett.* **100**, 227602 (2008).

[17] de Groot, F. M. F. X-ray absorption and dichroism of transition metals and their compounds. *J. Electron Spectrosc. Relat. Phenom.* **67**, 529 (1994).

[18] Chen, C. T. *et al.* Soft-X-ray magnetic circular-dichroism at the $L_{2,3}$ edges of nickel. *Phys. Rev. B* **42**, 7262 (1990).

[19] Hatt, A. J., Spaldin, N. A., and Ederer, C. Strain-induced isosymmetric phase transition in $BiFeO_3$. *Phys. Rev. Lett.* **81**, 054109 (2010).

[20] Lu, Y. X. *et al.* Epitaxial growth and magnetic properties of half-metallic Fe_3O_4 on GaAs(100). *Phys. Rev. B* **70**, 2333-4 (2004).

[21] Morrall, P. *et al.* Stoichiometry of $Fe_{3-\delta}O_4$(111) ultrathin films on Pt(111). *Phys. Rev. B* **67**, 214408 (2003).

[22] Koide, T. *et al.* Close correlation between the magnetic moments, lattice distortions, and hybridization in $LaMnO_3$ and $La_{1-x}Sr_xMnO_{3+\delta}$: doping dependent magnetic circular x-ray dichroism study. *Phys. Rev. Lett.* **87**, 246404 (2001).

[23] Chakhalian, J. *et al.* Magnetism at the interface ferromagnetic and superconducting oxides. *Nature Physics* **2**, 244 (2006).

[24] Moriya, T. Anisotropic superexchange interaction and weak ferromagnetism. *Phys. Rev.* **120**, 91-96 (1960).

[25] Phillips, T. G., Townsend, Jr., R. L., and White, R. L. Piezomagnetism of CoF_2 and α-Fe_2O_3 from electron-paramagnetic-resonance pressure experiments. *Phys. Rev. Lett.* **18**, 646-647 (1967).

[26] Borovik-Romanov, A. S. Piezomangetism, linear magnetostriction and magnetooptic effect. *Ferroelectrics* **162**, 153-159 (1994).

[27] Chu, Y.-H. *et al.* Electric-field control of local ferromagnetism using a magnetoelectric multiferroic. *Nature Mater.* **7**, 478 (2008).

Figure captions:

Figure 1. **Understanding the structures of different phases in mixed phase $BiFeO_3$ thin films**. (a) Large scale atomic force microscopy topography image of mixed phase BFO sample. Red and green shaded areas are two orthogonal sets of mixed phase features. (b) High resolution atomic force microscopy topography image of a mixed phase structure and cross section line profile of the white line. R- and T-phases shows two different slopes of ~1.6° and ~2.8°. (c) X-ray diffraction 2θ-ω map of a mixed phase film. (d) Schematic of T/R mixed phase structure.

Figure 2. **X-ray magnetic circular dichroism study of mixed phase, pure rhombohedral phase, and pure tetragonal phase films.** (a) XMCD spectra of three different kinds of films probed with fixed X-ray circular polarization (right circularly polarized) and alternated external magnetic field of magnitude 2 T. (b) XMCD spectra of three different kinds of films measured with X-ray polarization switched between right circular and left circular in constant magnetic field of 4 T.

Figure 3. **Photo-emission electron microscopy imaging of mixed phase film.** (a) Schematic of geometry of the measurements. The X-ray comes in at a grazing incidence, alternating between left and right circular polarization. Yellow, green, and blue arrows are X-rays coming in from different orientations, resulting from the rotation of the sample, which are 90° away from the neighbors. (b) PEEM image on the left side is taken with left circularly polarized X-rays giving mainly structural contrast. Darker stripes are R-phase and bright areas are the T-phase. XMCD PEEM image on the right side showing enhanced magnetic contrast is given from the ratio of PEEM images taken with left and right circularly polarized X-rays at the same location. Black

and white contrasts indicate magnetic moments pointing parallel and anti-parallel to the incident X-rays. (c) XMCD PEEM image, showing reversed magnetic contrast, is taken with 180° sample rotation from images in (b). (d) Upper and lower XMCD PEEM images are taken with 90° and 180° sample rotations from image (b).

Figure 4. **Detailed PEEM and PFM analysis of a mixed phase structure.** (a)-(c) Corresponding AFM topography, PFM, zoomed-in XMCD-PEEM image of the red-boxed area in Fig. 3(b). (d) Superimposed line profiles of the black, green, and red lines in Figure (a)-(c). Red bars locate the enhanced magnetic moment, where the magnitude of XMCD signal reaches its maxima (minima in XMCD curve). R- and T-phases are labeled next to their corresponding slopes.

Figure 5. **Exchange interaction between $Co_{.90}Fe_{.10}$ layer and mixed phase $BiFeO_3$ films beneath.** (a) LCP-PEEM image of CoFe layer on mixed phase BFO film showing topographic contrast. The green arrow illustrates the direction of applied magnetic field during CoFe growth. (b)-(e) XMCD-PEEM image given from the ratio of LCP and RCP-PEEM images of the same area, showing magnetic contrast of CoFe domains. White, black, and neutral gray contrasts indicate magnetic moment pointing parallel, antiparallel, and perpendicular to the incident X-rays. The direction of incident X-rays are marked as orange arrows. (f) Schematic of magnetic domains in CoFe (wide yellow and purple bars), which simulates the CoFe domain structures of the red-boxed area in (a) and (b), coupled with the mixed phase structure (thin dark ovals) beneath. Magnetic moment of CoFe domains are shown as white arrows.

Figure 6. **Illustration of electrical control of magnetism in mixed phase $BiFeO_3$ thin films.** (a) LCP PEEM image of a box-in-box electrically switched area, where the mixed phase stripes are erased in the red box scanned with a PFM tip at +24V DC bias and returned in the green box with -8V DC bias. (b) XMCD PEEM image of the switched area showing magnetic contrast from the mixed phase structures. The magnetic moments between the red and green boxes are turned off by the electric field and the magnetic moments in the green box are turned on again.

Figures

Figure 1.

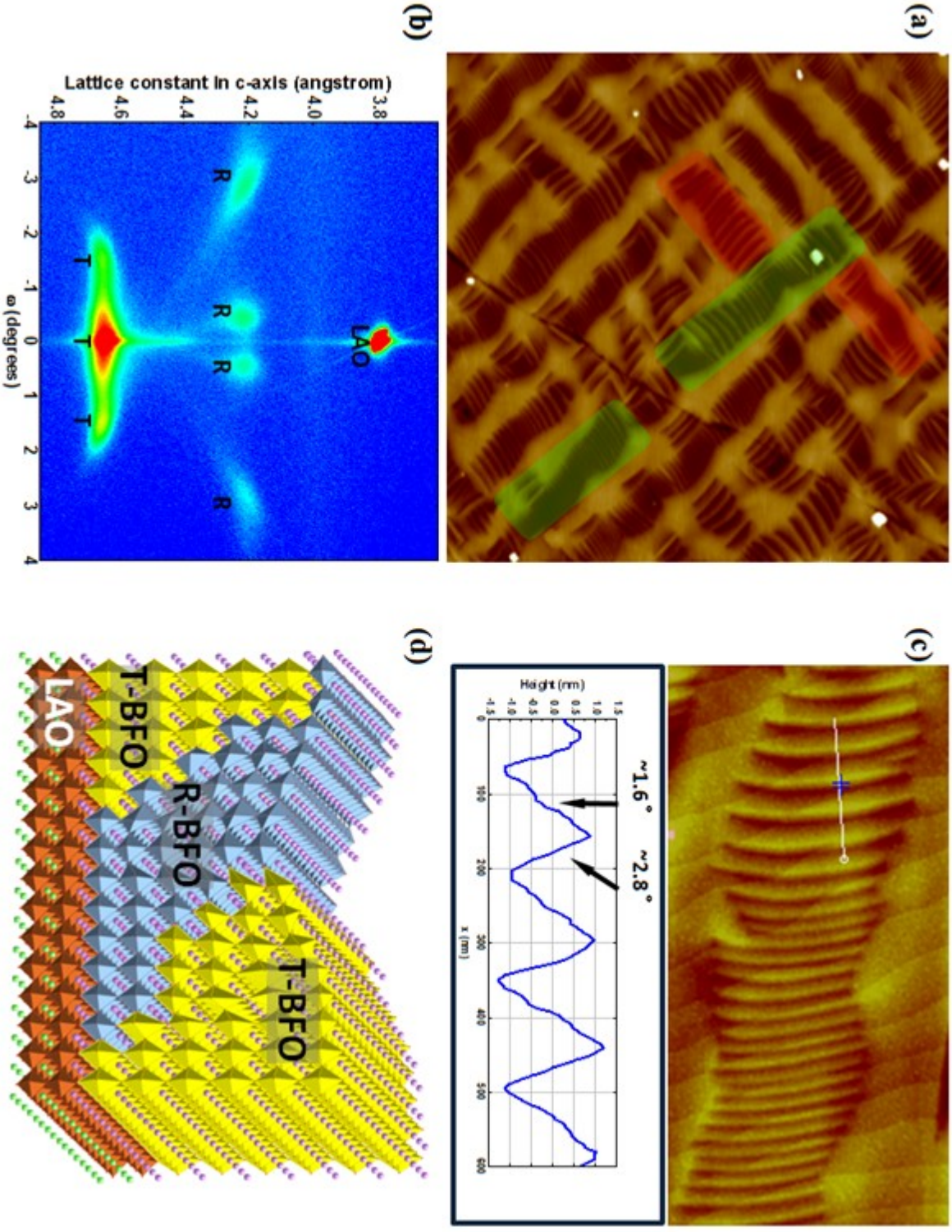

Figure 2.

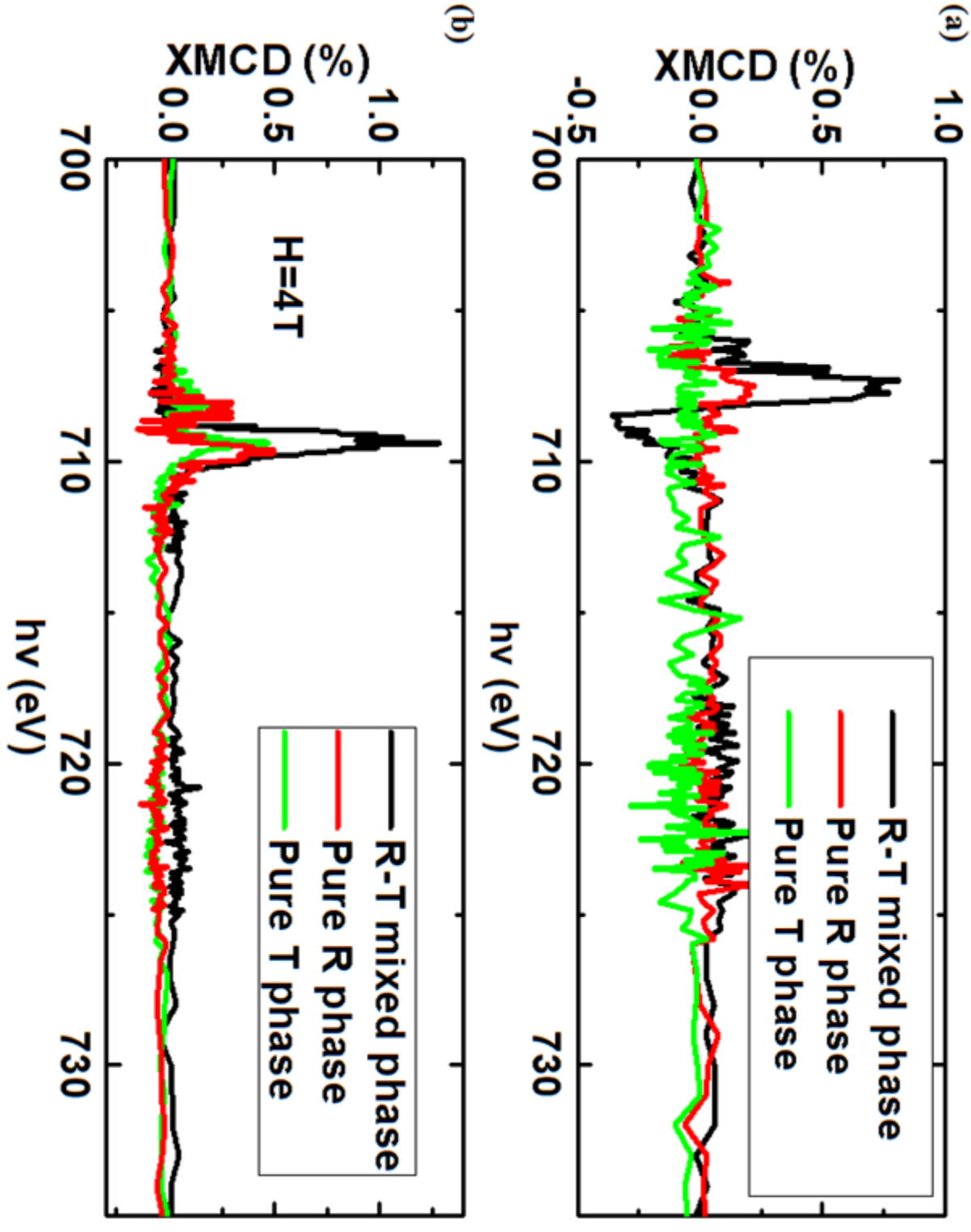
(a)
XMCD (%)
1.0
0.5
0.0
-0.5
700
710
720
730
hv (eV)
R-T mixed phase
Pure R phase
Pure T phase
(b)
XMCD (%)
1.0
0.5
0.0
H=4T
700
710
720
730
hv (eV)
R-T mixed phase
Pure R phase
Pure T phase

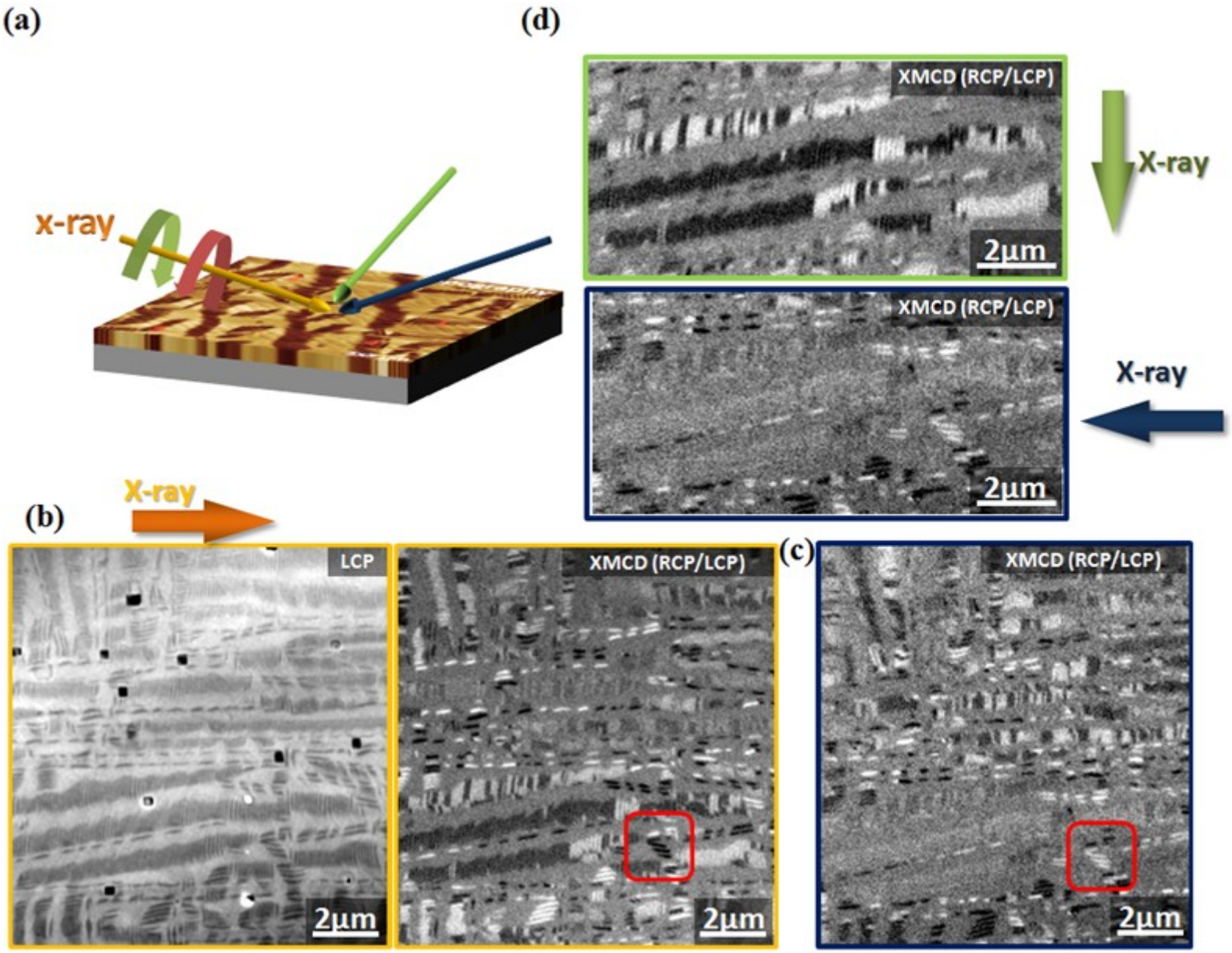
(a)
x-ray
(d)
XMCD (RCP/LCP)
2µm
X-ray
XMCD (RCP/LCP)
2µm
X-ray
(b)
X-ray
LCP
2µm
XMCD (RCP/LCP)
2µm
(c)
XMCD (RCP/LCP)
2µm

Figure 3.

Figure 4.

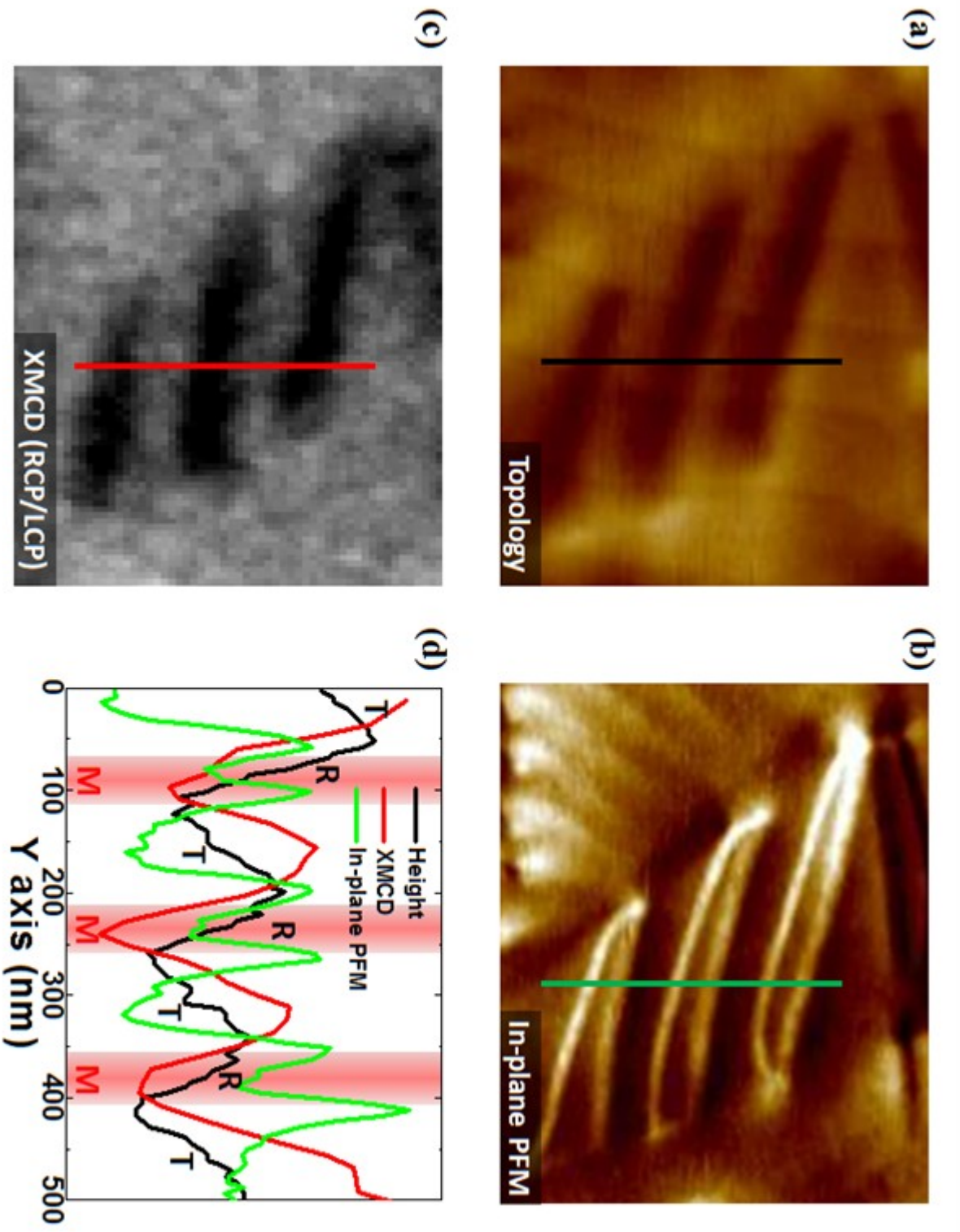
(a)
Topology
(b)
In-plane PFM
(c)
XMCD (RCP/LCP)
(d)
Height
XMCD
In-plane PFM
T
R
M
T
R
M
T
R
M
T
0
100
200
300
400
500
Y axis (nm)

Figure 5.

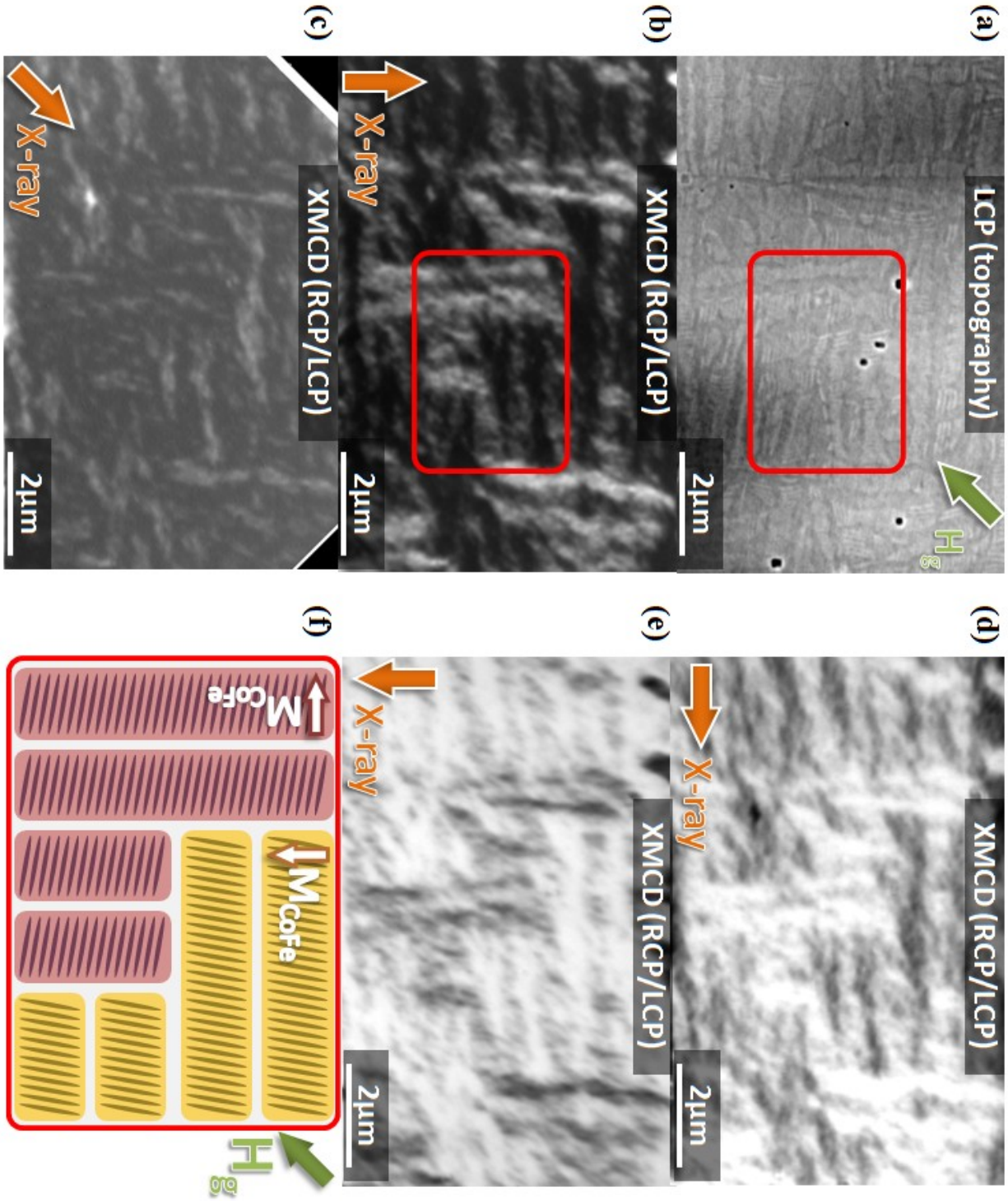
(a)
LCP (topography)
2µm
(b)
XMCD (RCP/LCP)
2µm
(c)
X-ray
XMCD (RCP/LCP)
2µm
X-ray
(d)
XMCD (RCP/LCP)
2µm
(e)
X-ray
XMCD (RCP/LCP)
2µm
X-ray
(f)
M_CoFe
M_CoFe

Figure 6.